Redox Biology 55 (2022) 102413

Contents lists available at ScienceDirect

Redox Biology

journal homepage: www.elsevier.com/locate/redox

NCOA4-mediated ferritinophagy is involved in ionizing radiation-induced ferroptosis of intestinal epithelial cells

Hao Zhou [a,1], Ya-Li Zhou [b,1], Jiu-Ang Mao [c,1], Lin-Feng Tang [a], Jie Xu [b], Zhen-Xin Wang [c,***], Yang He [b,**], Ming Li [a,*]

[a] State Key Laboratory of Radiation Medicine and Protection, School of Radiation Medicine and Protection, Medical College of Soochow University, Collaborative Innovation Center of Radiation Medicine of Jiangsu Higher Education Institutions, Soochow University, Suzhou, 215123, China
[b] MOE Engineering Center of Hematological Disease, Jiangsu Institute of Hematology, First Affiliated Hospital of Soochow University, Cyrus Tang Hematology Center, Collaborative Innovation Center of Hematology, Soochow University, Suzhou, 215006, China
[c] Department of Medical Oncology, The First Affiliated Hospital of Soochow University, Suzhou, 215006, China

ARTICLE INFO

Keywords:
Ferroptosis
Ferritinophagy
Intestinal epithelial cells
Ionizing radiation
Reactive oxygen species (ROS)

ABSTRACT

Ferroptosis is a newly recognized form of regulated cell death that is characterized by severe lipid peroxidation initiated by iron overload and the generation of reactive oxygen species (ROS). However, the role of iron in ionizing radiation (IR)-induced intestinal injury has not been fully illustrated yet. In this study, we found that IR induced ferroptosis in intestinal epithelial cells, as indicated by the increase in intracellular iron levels and lipid peroxidation, upregulation of prostaglandin-endoperoxide synthase 2 (PTGS2) mRNA, reduced glutathione peroxidase 4 (GPX4) mRNA and glutathione (GSH) levels, and significant mitochondrial damage. In addition, the iron chelator deferoxamine (DFO) attenuated IR-induced ferroptosis and intestinal injury *in vitro* and *in vivo*. Intriguingly, pharmacological inhibition of autophagy with 3-methyladenine (3-MA) mitigated IR-induced ferritin downregulation, iron overload and ferroptosis. IR increased the levels of nuclear receptor coactivator 4 (NCOA4) mRNA and protein. NCOA4 knockdown significantly inhibited the reduction of ferritin, decreased the level of intracellular free iron, and mitigated ferroptosis induced by IR in HIEC cells, indicating that NCOA4-mediated autophagic degradation of ferritin (ferritinophagy) was required for IR-induced ferroptosis. Furthermore, cytoplasmic iron further activated mitoferrin2 (Mfrn2) on the mitochondrial membrane, which in turn increased iron transport into the mitochondria, resulting in increased ROS production and ferroptosis. In addition, mice fed with an iron-deficient diet for 3 weeks showed a significant reversal in the intestinal injury induced by abdominal IR exposure. Taken together, ferroptosis is a novel mechanism of IR-induced intestinal epithelial cytotoxicity, and is dependent on NCOA4-mediated ferritinophagy.

1. Introduction

The small intestinal mucosa is highly sensitive to ionizing radiation (IR). Systemic radiation exposure and radiotherapy for abdominal and pelvic tumors can cause significant damage to the small intestine. The incidence of radiation-induced intestinal injury (RIII) is relatively high among abdominal and pelvic tumor patients undergoing radiotherapy. Almost 60–80% of the patients show transient intestinal toxicity

Abbreviations: ROS, reactive oxygen species; IR, ionizing radiation; PTGS2, prostaglandin-endoperoxide synthase2; GPX4, glutathione peroxidase 4; GSH, glutathione; NCOA4, nuclear receptor coactivator 4; Mfrn2, mitoferrin2; RIII, radiation-induced intestinal injury; FTH, ferritin heavy chain; FTL, ferritin lightchain; TfR1, transferrin receptor 1; FPN1, ferriportin 1; MDA, malondialdehyde; TAI, total abdominal irradiation; Ftmt, ferritin mitochondrial; ID, iron-deficient diet; ND, normal diet; RBC, red blood cells; Hb, hemoglobin; IRP, iron regulatory protein; Nrf2, nuclear factor E2-related factor 2; ATG, autophagy related gene; ISCs, intestinal stem cells.

* Corresponding author. School of Radiation Medicine and Protection, Medical College of Soochow University, Ren'ai Road 199, Suzhou, 215123, China.
** Corresponding author. MOH Key Lab of Thrombosis and Hemostasis, Jiangsu Institute of Hematology, The First Affiliated Hospital of Soochow University, Shizi street 188, Suzhou, 215006, China.
*** Corresponding author. Department of Medical Oncology, The First Affiliated Hospital of Soochow University, Shizi street 188, Suzhou, 215006, China.
E-mail addresses: zhenxw316@163.com (Z.-X. Wang), heyang1963@163.com (Y. He), lim1984@suda.edu.cn (M. Li).
[1] These authors have contributed equally to this work and share first authorship.

https://doi.org/10.1016/j.redox.2022.102413
Received 30 June 2022; Received in revised form 14 July 2022; Accepted 16 July 2022
Available online 30 July 2022

symptoms during radiotherapy, and 50% experience some degree of chronic intestinal dysfunction. Furthermore, radiation enteropathy is one of the most common side effects among long-term cancer survivors [1]. Despite recent research progress, the mechanisms underlying the pathogenesis of RIII and the effect of radioprotective drugs remain largely unknown, resulting in the lack of effective prevention and treatment methods. Therefore, there is an urgent need to explore the pathogenic basis of RIII.

IR-induced death of the rapidly proliferating intestinal crypt cells is considered to be the major cause of RIII [2]. Radiation exposure can trigger apoptosis, necrosis, autophagy and mitotic catastrophe in mammalian cells [3], although the predominant form of IR-induced cell death is currently unclear. Lei G et al. [4] and Ye LF et al. [5] showed that IR can induce ferroptosis, an iron-dependent non-apoptotic form of cell death characterized by intracellular accumulation of reactive oxygen species (ROS) [6], in tumor cells. Ferroptosis is morphologically, biochemically and genetically different from other types of cell death. Cells undergoing ferroptosis are morphologically characterized by shrunken mitochondria with increased membrane density, few or absent cristae and ruptured outer membrane. In addition, increased iron deposition and lipid peroxidation, as well as overexpression of key genes/proteins involved in lipid metabolism such as prostaglandin-endoperoxide synthase 2 (PTGS2) and acyl-CoA synthetase long-chain family member 4 (ACSL4), are other cardinal features of ferroptosis. Ferroptosis is associated with degenerative diseases (e.g., Alzheimer's disease, Huntington's disease and Parkinson's disease), carcinogenesis, stroke, cerebral hemorrhage, traumatic brain injury, ischemic reperfusion injury and kidney degeneration-related pathological cell death in mammals, and the progression of these diseases can be mitigated by activation or inhibition of ferroptosis pathways [7,8].

Studies show that IR can induce ferroptosis in normal lung tissues [9], myeloid-macrophage progenitor cells [10] and intestinal epithelial cells [11], and ferroptosis inhibitors can protect against IR-induced lung injury [12], hematopoietic damage [13] and intestinal injury [11]. Furthermore, ferroptosis inhibitors alone or in combination with anti-apoptotic and anti-necrosis drugs can significantly improve the survival of lethally irradiated mice [10,14]. However, the exact mechanism of IR-induced ferroptosis of intestinal epithelial cells is still unclear. The ferroptosis inhibitor ferrostatin-1 (Fer-1) can reduce IR-induced cell death by blocking the lipid peroxidation pathway without repairing DNA damage [4,5]. This suggests that along with DNA damage, lipid peroxidation also plays an important role in radiation-induced cell death.

Since ferroptosis is induced by iron overload and excessive production of ROS, iron metabolism is one of the key influencing factors [7]. Iron is an essential trace element that is widely distributed in nearly all tissues of the human body. It is the primary building block of hemoglobin and myoglobin, as well as a cofactor for many key enzymes in redox reactions. Nevertheless, excessive amounts of intracellular free iron can generate high levels of free radicals through Fenton and Haber-Weiss reactions, which in turn cause oxidative damage to membrane lipids, proteins and DNA, eventually resulting in cell death. Therefore, it is critical to maintaining intracellular iron homeostasis, which depends on the coordination between iron absorption, transport and storage. As the only organ of dietary iron absorption and the temporary organ of iron storage, the small intestine plays an important role in iron metabolism. Most studies on the pathogenic basis of RIII have focused on IR-induced DNA damage, especially DNA double-strand breaks and the resulting apoptosis, whereas the roles of intestinal and dietary iron are still unclear.

In a previous study, we found that IR triggered ROS production and lipid peroxidation in the human intestinal epithelial cell line HIEC. Furthermore, the antioxidant and ferroptosis inhibitor (−)-epigallocatechin-3-gallate (EGCG) eliminated ROS, reduced lipid peroxidation and upregulated the anti-ferroptosis protein solute carrier family 7 member 11 (SLC7A11) [15]. However, the pathways employed by IR to induce ferroptosis in intestinal epithelial cells are not known. In this study, we explored the specific mechanisms underlying IR-induced ferroptosis in intestinal epithelial cells, and examined the impact of IR on intestinal iron content, as well as the potential role of intestinal and dietary iron on the progression of RIII.

2. Materials and methods

2.1. Antibodies and reagents

Primary antibodies for Western blotting included anti-ferritin heavy chain (FTH, 1:1000), anti-ferritin light chain (FTL, 1:5000), anti-transferrin receptor 1 (TfR1, 1:1000) (all from Abcam, Cambridge, UK), anti-nuclear receptor coactivator 4 (NCOA4, 1:1000; Invitrogen, Carlsbad, CA, USA), anti-ferriportin 1 (FPN1, 1:1000) and anti-tubulin (1:1000; Proteintech, Rosemont, IL, USA). Anti-NCOA4 (1:200), anti-glutathione peroxidase 4 (GPX4, 1:350; Abcam, Cambridge, UK) and anti-Ki67 antibodies (1:500; Cell Signaling Technologies, Beverly, MA, USA) were used for immunohistochemical staining. Deferoxamine (DFO), Fer-1 and N-acetyl-L-cysteine (NAC) were purchased from Sigma-Aldrich (St Louis, MO, USA). Necrostatin-1 (Nec-1) was obtained from Abcam (Cambridge, UK). Ferric amine citrate (FAC) was purchased from Yuanye Biotec (Shanghai, China) and 3-methyladenine (3-MA) from Medchem Express (Monmouth Junction, NJ, USA). FerroOrange and Mito-FerroGreen fluorescence probe were purchased from Dojindo Laboratories (Kumamoto, Japan). Liproxstatin-1 (Lip-1), BODIPY™ 581/591C11 and MitoSOX™ Red fluorescence probe were bought from Thermo Fisher Scientific (Waltham, MA, USA). Z-VAD, Cell counting kit 8 (CCK-8), ATP assay kit, Mito-Tracker Red CMXRos, GSH and GSSG Assay kit, bicinchoninic acid (BCA) protein assay kit, mitochondrial transmembrane potential assay kit with JC-1 and Hoechst 33342 were from Beyotime Institute of Biotechnology (Shanghai, China). Mounting medium with DAPI (4′,6-diamidino-2-phenylindole), ready-to-use HRP-IgG dilutions and 3, 3N-diaminobenzidine tertrahydrochloride (DAB) kit were purchased from Zhongshan Golden Bridge Biotechnology (Beijing, China).

2.2. Cell culture and treatment

The human intestinal epithelial cell line HIEC was purchased from BeNa Culture Collection (Shanghai, China). The cells were cultured in Dulbecco's modified Eagle medium (DMEM) supplemented with 10% fetal bovine serum (FBS) and 1% (v/v) penicillin-streptomycin at 37 °C under 5% CO_2. The HIEC cells were pretreated with DFO (500 nM) for 24 h before radiation for cytoplasmic iron chelation, and with 3-MA (25 μM) to inhibit autophagy as per the experimental requirements. An *in vitro* model of intestinal epithelial cell injury was established by irradiating HIEC cells with a single dose of 6 Gy (as reported by Lei G et al. [4,16]) at the dose rate of 1.1 Gy/min using an X-RAD 320iX Biological Irradiator (Precision X-ray, North Branford, CT, USA). All *in vitro* experiments were repeated at least 3 times unless described otherwise.

2.3. Cell viability assay

The HIEC cells were seeded in replicates of 5 in 96-well plates at the density of 1000 cells/well, and incubated for 24 h. Cells were treated accordingly, and the medium was replaced with 100 μL fresh medium containing 10 μL CCK8 reagent. After incubating for 2 h, the optical density (OD) was measured using a microplate reader (BioTek Instruments, Inc., Winooski, VT, USA) at 450 nm.

2.4. Colony formation assay

The HIEC cells were seeded in triplicate in 6-well plates at the density of 100–800 cells/well depending on the radiation dose. After overnight culture, the cells were treated as required and the drug-supplemented

medium was replaced with fresh medium immediately post 0, 2, 4 or 6 Gy irradiation. The cells were cultured for 1–2 weeks and stained with crystal violet, and the viable colonies containing at least 50 cells were counted.

2.5. Transmission electron microscopy (TEM)

The cells were collected 24 h after irradiation and fixed with 2.5% glutaraldehyde at room temperature in the dark for 30 min. After dehydration and embedding in epoxy resin, ultrathin sections were prepared and examined under a transmission electron microscope (HITACHI, Tokyo, Japan).

2.6. Detection of iron in cells and tissues

FerroOrange was used to detect intracellular Fe^{2+} according to the manufacturer's protocols. The suitably treated HIEC cells were incubated with 1 μM FerroOrange in Hank's balanced salt solution (HBSS) for 30 min at 37 °C, and observed under a confocal laser scanning microscopy (Olympus Corp., Tokyo, Japan). To detect mitochondrial Fe^{2+}, HIEC cells were seeded in triplicate in 6-well plates, cultured overnight and treated with 0 or 500 nM DFO for 24 h before 0 or 6 Gy irradiation. The cells were incubated with 5 μM Mito-FerroGreen working solution for 30 min at 37 °C, and the presence of mitochondrial Fe^{2+} was observed under a fluorescence microscope (Olympus Corp., Tokyo, Japan).

The intestinal tissues were collected 3.5 days post radiation and freeze-dried, and 3 mg tissue per sample was digested overnight in 65% concentrated nitric acid. After removing nitric acid by heating, 1% nitric acid was added to equilibrate the volume to 1 mL. The concentration of iron in the tissues was measured by inductively coupled plasma mass spectrometer (ICP-MS, Thermo Fisher Scientific, Waltham, MA, USA).

2.7. Lipid peroxidation assay

The suitably treated cells were incubated with 5 μM BODIPY™ 581/591C11 fluorescence probe for 30 min in a humidified incubator (at 37 °C, 5% CO_2) and trypsinized to obtain a cell suspension. The lipid peroxidation levels were analyzed by flow cytometry (BD Bioscience, San Diego, CA, USA).

2.8. Mitochondrial ROS measurement

HIEC cells were plated in triplicate in 6-well plates, cultured overnight, and treated with 0 or 500 nM DFO for 24 h before 0 or 6 Gy irradiation. To measure mitochondrial superoxide levels, the cells were incubated with 5 μM MitoSOX probe for 10 min at 37 °C, washed with PBS, and observed under a fluorescence microscope (Olympus Corp., Tokyo, Japan).

2.9. ATP measurement

HIEC cells were seeded in triplicate in 6-well plates, cultured overnight, and treated with 0 or 500 nM DFO for 24 h before 0 or 6 Gy irradiation. The cellular ATP levels were measured using a firefly luciferase-based ATP assay kit according to the manufacturer's protocol. Briefly, the cells were centrifuged to remove any debris, and the supernatant was added to the substrate solution. The luminescence was recorded using a microplate reader (BioTek Instruments, Inc., Winooski, VT, USA).

2.10. Mitochondrial membrane potential measurement

HIEC cells were plated in triplicate in 6-well plates, cultured overnight, and treated with 0 or 500 nM DFO for 24 h before 0 or 6 Gy irradiation. Mitochondrial membrane potential (ΔΨm) in HIEC cells was assessed by ΔΨm assay kit with JC-1 according to the manufacturer's protocols. The decrease in ΔΨm was assessed by transition from JC-1 aggregates (red fluorescence) to JC-1 monomer (green fluorescence). The degree of mitochondrial dysfunction and early cell death was evaluated in terms of red/green fluorescence intensity ratio.

2.11. Mitochondrial morphology assessment

HIEC cells were seeded in 6-well plates in triplicate, cultured overnight, and treated with 0 or 500 nM DFO for 24 h before 0 or 6 Gy irradiation. The cells were stained with Mito-Tracker Red CMXRos according to the manufacturer's protocol and observed under a fluorescence microscope (Olympus Corp., Tokyo, Japan). The mitochondria were divided into the following three categories as previously described [17]: category I - elongated mitochondria organized in a tubular network; category II - large dotted mitochondria evenly distributed all over the cytosol; category III - totally fragmented mitochondria around the nucleus. At least 400 cells per sample were counted in a blinded manner.

2.12. Animals and animal model

All animal experiments were performed in accordance with the guidelines and protocols approved by the Animal Ethics Committee of Soochow University. Four to eight-week-old male C57BL/6J mice were purchased from Beijing Vital River Laboratory Animal Technology Co., Ltd, Shanghai Branch (Shanghai, China). The mice were housed in specific pathogen-free conditions under controlled ambient temperatures and humidity, with *ad libitum* access to food and water. The RIII model was established by 14 Gy (as reported by Wei L and Lu Q et al. [18,19]) total abdominal irradiation (TAI) using the X-RAD 320iX Biological Irradiator (Precision X-ray, North Branford, CT, USA) at the rate of 1.1 Gy/min. A 3-cm abdominal area covering the gastrointestinal tract was irradiated, and the other parts of the body were shielded. The mice in IR + DFO group were intraperitoneally injected with DFO (100 mg/kg) for 3 consecutive days before and 1 day after TAI (Fig. 3A). An equivalent volume of PBS was given intraperitoneally to the control mice. To induce iron deficiency, 4-weeks-old male C57BL/6J mice were fed an iron-deficient diet (TP0304, declared iron content 12 ppm; Trophic Animal Feed High-Tech Co., Ltd, Nantong, China) for 3 weeks. Control animals were fed the standard laboratory diet (TP0304C, iron content approximately 45 ppm).

2.13. MDA and GSH measurement

Small intestinal tissues were collected at 3.5 days post radiation. The content of malondialdehyde (MDA) and glutathione (GSH) was determined by Nanjing Jiancheng Bioengineering Institute (Nanjing, China). The level of GSH in HIEC cells was detected using a GSH and GSSG Assay kit following the manufacturer's instructions.

2.14. Histology and immunohistochemistry (IHC)

Small intestinal tissues were harvested at the indicated time points after irradiation and fixed overnight in 4% paraformaldehyde. After embedding in paraffin, 3 μm-thick sections were cut and stained with hematoxylin and eosin (H&E). Villus height was determined using Image J 1.53c software. IHC was performed as described in our previous publication [20].

2.15. Western blotting

Cultured cells were harvested at indicated time points. Protein extraction and Western blotting were performed according to published methods [21]. The expression levels of the target proteins were normalized to tubulin.

2.16. Quantitative real-time PCR (qRT-PCR)

QRT-PCR was performed as described in our previous study [21]. The expression levels of the target genes were normalized to β-actin. The primers are listed in Supplementary Table 1 and were synthesized by Sangon Biotech (Shanghai, China).

2.17. Small interfering RNA (siRNA) and transfection

NCOA4 and Mfrn2-targeting siRNAs (siNCOA4 and siMfrn2) or non-targeting control siRNAs (siNC) were synthesized by GenePharm (Shanghai, China). The sequences are listed in Supplementary Table 2. HIEC cells in the logarithmic growth phase were seeded in 3.5 cm culture dishes and transiently transfected with 20 μM siNCOA4, siMfrn2 or siNC using Lipofectamine 3000 (Invitrogen, Carlsbad, CA, USA) according to the manufacturer's instructions. Cells were harvested 48 h after transfection, and total cellular protein or mRNA was extracted for western blotting and qRT-PCR respectively.

2.18. Statistical analysis

The data were presented as means ± standard deviation (S.D.), analyzed and visualized using ggplot2 in R version 3.6.3. Kaplan-Meier analysis was used to assess the survival rate, and the survival curves were plotted by GraphPad Prism 6.0 (San Diego, CA, USA). Two groups were compared by Student's *t*-test and multiple groups were compared by one-way analysis (ANOVA) of variance followed by Tukey's post hoc test. *P* values < 0.05 were considered statistically significant.

3. Results

3.1. IR induced iron overload and ferroptosis in intestinal epithelial cells

To determine whether IR could induce ferroptosis in intestinal epithelial cells, HIEC cells were irradiated with 6 Gy IR. We detected a significant increase in intracellular Fe^{2+} levels at 12 h post-irradiation, and the iron overload gradually increased with time (Fig. 1A). Furthermore, lipid peroxidation also increased significantly in the irradiated HIEC cells in a time-dependent manner (Fig. 1B). Consistent with the above, the ferroptosis marker PTGS2 (mRNA) was significantly

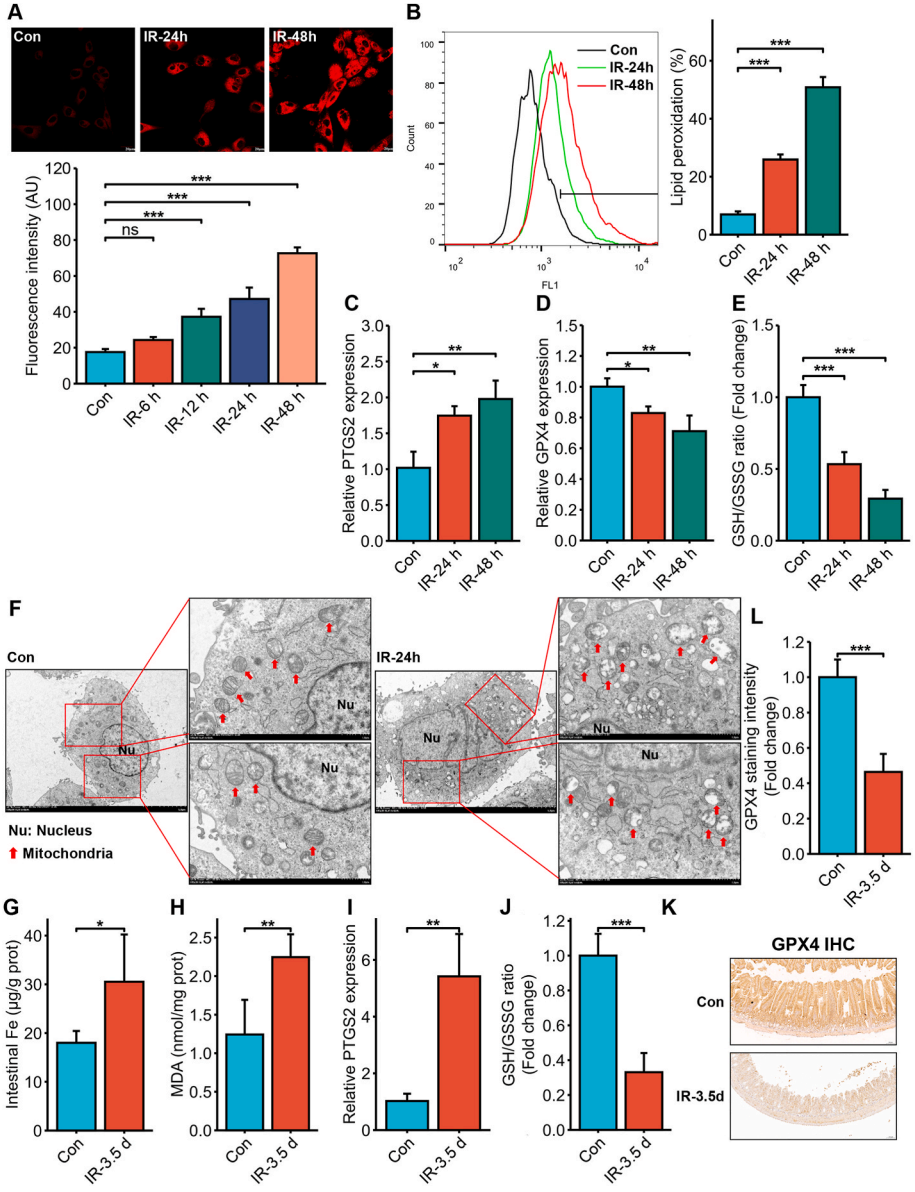

Fig. 1. IR induced intracellular iron overload and ferroptosis in intestinal epithelial cells *in vitro* and *in vivo*. (A) Representative images of FerroOrange-stained HIEC cells showing intracellular Fe^{2+} levels 6, 12, 24 and 48 h post exposure to 6 Gy IR. Scale bar = 20 μm. Bar graph showing fluorescence intensity in the indicated cells. n = 3 independent experiments. (B) Representative images of C11-BODIPY-stained HIEC cells showing lipid peroxidation 24 and 48 h after 6 Gy IR. Bar graph showing relative levels of lipid peroxidation in the indicated cells. n = 3 independent experiments. (C) PTGS2 mRNA levels in the HIEC cells 24 and 48 h after 6 Gy IR. n = 3 independent experiments. (D) GPX4 mRNA levels in the HIEC cells 24 and 48 h after 6 Gy IR. n = 3 independent experiments. (E) Glutathione (GSH) levels in HIEC cells 24 and 48 h after 6 Gy IR. n = 3 independent experiments. (F) Representative TEM images of HIEC cells showing the ultrastructure of mitochondria 24 h after 6 Gy IR (the magnification is shown in the picture). The red arrow indicates mitochondria. Bar graphs showing Fe (G), malondialdehyde (MDA) (H), PTGS2 mRNA (I) and GSH (J) levels in the small intestinal tissues of C57BL/6J mice 3.5 days post 14 Gy TAI. n = 5 per group. (K) Representative IHC images of intestinal sections of C57BL/6J mice at 3.5 days after 14 Gy TAI showing GPX4 expression (Scale bar = 100 μm). (L) Quantitative analysis of GPX4 staining. All data are presented as mean ± S.D. ns, $p \geq 0.05$; *, $p < 0.05$; **, $p < 0.01$; ***, $p < 0.001$. (For interpretation of the references to colour in this figure legend, the reader is referred to the Web version of this article.)

upregulated (Fig. 1C) whereas the levels of the antioxidant glutathione peroxidase 4 (GPX4) mRNA and glutathione (GSH) were significantly decreased (Fig. 1D and E) in the irradiated cells in a time-dependent manner. Furthermore, transmission electron microscopy showed reduced or absent mitochondrial cristae and ruptured outer membrane in the HIEC cells 24 h post-irradiation, which are the characteristic morphological features of ferroptosis (Fig. 1F). Taken together, IR induced iron overload and triggered ferroptosis in HIEC cells.

To confirm that IR induced ferroptosis *in vivo*, C57 mice were subjected to 14 Gy TAI and intestinal tissue samples were harvested 3.5 days post-irradiation. ICP-MS revealed a significant increase in iron concentration in the intestines of the irradiated mice (Fig. 1G), which is indicative of IR-induced iron overload. In addition, the lipid peroxidation marker malondialdehyde (MDA, Fig. 1H) and PTGS2 mRNA (Fig. 1I) showed a significant increase, while GSH (Fig. 1J) and GPX4 levels (Fig. 1K and L) were significantly decreased after irradiation. Thus, IR induced ferroptosis in mouse intestines, which was consistent with the *in vitro* results.

IR can induce several forms of cell death including apoptosis, necrosis and autophagy [3]. While these forms of cell death may coexist in the same pathological situation, their contributions vary considerably [22]. To determine the primary form of death in the HIEC cells post-irradiation, we pre-treated the cells with the iron chelator DFO, or inhibitors of ferroptosis (Fer-1), necroptosis (Nec-1), apoptosis (Z-VAD) or autophagy (3-MA), and exposed them to 6 Gy IR. According to the CCK-8 and clonogenic assays, Fer-1, DFO and 3-MA significantly reduced IR-induced cell death. In contrast, Nec-1 and Z-VAD increased the viability of irradiated cells, while their clonogenic potential was not improved (Supplementary Figure 1). Taken together, IR can induce intestinal iron overload and ferroptosis *in vitro* and *in vivo*, and ferroptosis and autophagy are the predominant modes of IR-induced intestinal cell death.

3.2. Decreased intracellular iron levels protected intestinal epithelial cells against IR-induced ferroptosis

To further determine the role of iron in the progression of RIII, we pre-treated HIEC cells with DFO to decrease intracellular iron concentration and exposed the cells to 6 Gy IR. As shown in Fig. 2A, intracellular Fe^{2+} levels increased significantly after irradiation and were effectively inhibited by DFO pre-treatment. Compared to the untreated cells, the DFO-treated cells also had lower lipid peroxidation (Fig. 2B) and PTGS2 mRNA expression (Fig. 2C), along with increased GPX4 and GSH levels (Fig. 2D and E) after irradiation, indicating that the iron concentration in the irradiated HIEC cells is closely associated with ferroptosis. Furthermore, DFO pre-treatment increased the survival and clonogenic potential of irradiated HIEC cells (2, 4 or 6 Gy) compared to that of the non-irradiated controls, especially in the 2 Gy dose group (Fig. 2F). Thus, DFO-mediated reduction in intracellular iron levels decreased ferroptosis and increased the survival of HIEC cells.

To confirm the role of iron in RIII *in vivo*, we intraperitoneally injected C57BL/6J mice with 100 mg/kg DFO and subjected them to 14 Gy TAI (Fig. 3A). As shown in Fig. 3B, the irradiation-induced iron accumulation in the intestines was significantly inhibited by DFO pre-treatment. DFO treatment significantly improved the survival of the lethally irradiated mice compared to that of the vehicle-treated mice

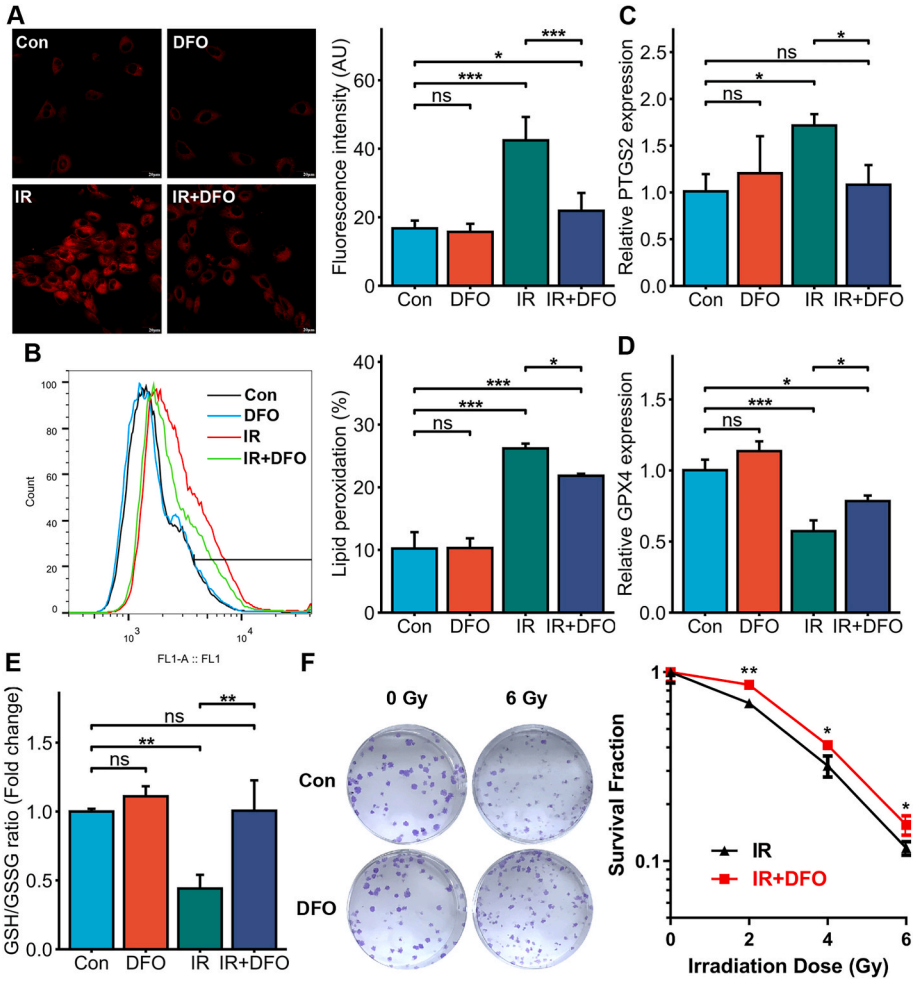

Fig. 2. The iron chelator deferoxamine (DFO) alleviated IR-induced ferroptosis in HIEC cells. (A) Representative images of FerroOrange-stained control or DFO (500 nM)-treated HIEC cells after 0 or 6 Gy IR showing intracellular Fe^{2+}. Scale bar = 20 μm. Bar graph showing fluorescence intensity in the indicated cells. n = 3 independent experiments. (B) Representative images of C11-BODIPY-stained control or DFO (500 nM)-treated HIEC cells after 0 or 6 Gy IR and bar graph showing relative levels of lipid peroxidation in the indicated cells. n = 3 independent experiments. (C) PTGS2 mRNA levels in the control or DFO (500 nM)-treated HIEC cells after 0 or 6 Gy IR. n = 3 independent experiments. (D) GPX4 mRNA levels in the control or DFO (500 nM)-treated HIEC cells after 0 or 6 Gy IR. n = 3 independent experiments. (E) GSH levels in the control or DFO (500 nM)-treated HIEC cells after 0 or 6 Gy IR. n = 3 independent experiments. (F) Representative images of colonies formed by the control or DFO (500 nM)-treated HIECs exposed to 0 or 6 Gy IR and the survival curve of the cells exposed to 0, 2, 4 or 6 Gy IR. n = 3 independent experiments. All data are presented as mean ± S.D. ns, $p \geq 0.05$; *, $p < 0.05$; **, $p < 0.01$; ***, $p < 0.001$.

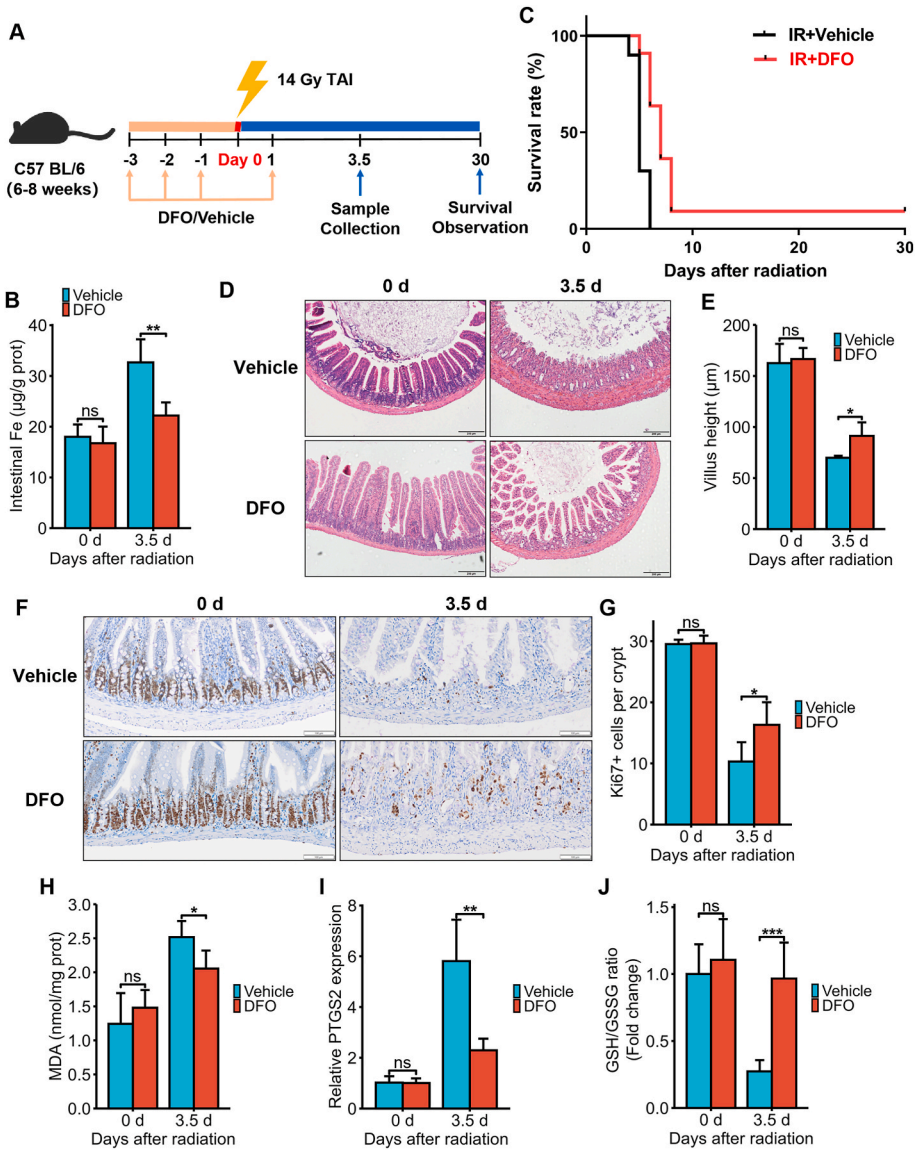

Fig. 3. DFO treatment alleviated IR-induced ferroptosis and intestinal injury in C57BL/6J mice exposed to 14 Gy TAI. (A) Experimental scheme. The mice were intraperitoneally injected with vehicle (PBS) or DFO (100 mg/kg) for 3 consecutive days before and 1 day after 14Gy TAI. Small intestinal samples were collected 3.5 days post-TAI. Survival of irradiated mice was monitored for up to 30 days post-TAI. (B) Intestinal Fe content of vehicle (PBS) or DFO (100 mg/kg)-treated mice at days 0 and 3.5 after 14 Gy TAI as determined by ICP-MS. (C) Kaplan-Meier survival curves of C57BL/6J mice (n = 10 for IR + Vehicle group and n = 11 for IR + DFO group). (D) Representative images of H&E-stained intestinal sections from vehicle or DFO-treated mice at days 0 and 3.5 after 14 Gy-TAI (Scale bar = 200 μm). (E) Bar graph comparing villus heights in different groups (n = 5/group). All villi around a circumference were measured per sample. (F) Representative IHC images of intestinal sections of vehicle and DFO-treated mice at 3.5 days after TAI showing Ki67 expression (Scale bar = 100 μm). (G) Histograms showing number of Ki67^{+} cells per crypt determined from panel (F) (n = 5/group). Bar graph showing the levels of MDA (H), PTGS2 mRNA (I) and GSH (J) in small intestinal tissues of C57BL/6J mice at 3.5 days post 14 Gy TAI. n = 5 for each treatment. All data are presented as mean ± S.D. ns, $p \geq 0.05$; *, $p < 0.05$; **, $p < 0.01$; ***, $p < 0.001$.

over a period of 30 days ($p = 0.0005$, IR + Vehicle: 0% *v.s.* IR + DFO: 9.1%, Fig. 3C). In addition, although villus height decreased significantly in both groups on day 3.5 post-TAI, it was still markedly greater in the DFO-treated group than the vehicle-treated group (Fig. 3D and E). Consistent with this, the *in-situ* expression of Ki67 protein in the small intestinal tissues (Fig. 3F) and the mean number of Ki67^{+} cells in the crypts (Fig. 3G) decreased significantly 3.5 days post-TAI but was markedly restored by DFO pre-treatment. To assess the impact of DFO on intestinal cell ferroptosis, we measured MDA, PTGS2 and GSH levels in the tissues on day 3.5 post-TAI. Compared to the vehicle group, mice in the DFO group had significantly lower MDA content (Fig. 3H) and PTGS2 mRNA levels (Fig. 3I) along with higher GSH levels (Fig. 3J), suggesting that DFO can mitigate IR-induced ferroptosis in small intestinal cells and the ensuing tissue injury. Taken together, a reduction in the content of iron in intestinal epithelial cells protected the cells against ferroptosis and RIII *in vitro* and *in vivo*.

3.3. Intracellular iron overload promoted ferroptosis and increased the radiosensitivity of intestinal epithelial cells

Although the radiosensitizing effects of iron on tumor cells are well recognized [23], its role in normal intestinal tissues has rarely been investigated. Therefore, we treated HIEC cells with ferric ammonium citrate (FAC) to increase intracellular iron concentration prior to IR exposure (Supplementary Figure 2A). Our results indicated that FAC or IR exposure alone led to mild lipid peroxidation, whereas co-treatment with FAC and IR led to significant lipid peroxidation in the HIEC cells ($p < 0.001$, Supplementary Figure 2B). This suggests that FAC can augment IR-induced lipid peroxidation in HIEC cells. Furthermore, the combination of FAC and IR significantly decreased the viability of HIEC cells compared to that in the control and FAC/IR groups ($p < 0.001$, Supplementary Figure 2C). The ferroptosis inhibitor liproxstatin-1 (Lip-1) and DFO effectively reversed the FAC-induced lipid peroxidation and reduction in cell viability. Taken together, iron overload in intestinal epithelial cells promoted IR-induced ferroptosis and increased radiosensitivity.

Previous studies have shown that crypts isolated from the small intestine can form intestinal organoids in 3D Matrigel scaffolds *in vitro* in the presence of growth factors [24]. We irradiated mouse small intestinal crypt organoids with 8 Gy IR, and analyzed crypt growth and surface area. Our results showed that FAC significantly inhibited crypt growth and increased the radiosensitivity of the organoids, which was reversed by DFO treatment (Supplementary Figure 2D, E).

3.4. Ferritinophagy was involved in IR-induced intracellular iron overload

To further explore the mechanisms through which IR induced iron overload in the intestinal epithelial cells, we analyzed the changes in the expression levels of iron regulatory proteins including transferrin receptor 1 (TfR1) (iron input), ferroportin 1 (FPN1) (iron output), ferritin heavy chain (FTH) and ferritin light chain (FTL) (iron storage) at different time points post-irradiation (6 Gy). As shown in Fig. 4A, TfR1 was significantly upregulated, while FPN1, FTL and FTH were downregulated in the irradiated HIEC cells, indicating that the intracellular Fe^{2+} overload may be the result of increased iron input and reduced iron output and storage. A recent study identified ferritinophagy as a distinct form of autophagy that mediates ferritin degradation and releases free iron [25,26]. To confirm the involvement of ferritinophagy, we treated the cells with the autophagy inhibitor 3-MA prior to irradiation and measured ferritin (FTL and FTH) levels. As shown in Fig. 4B, both FTL and FTH were downregulated in the irradiated cells but upregulated in 3-MA-treated cells. Moreover, 3-MA also reversed the IR-induced increase in TfR1 (Fig. 4B). Consistent with this, 3-MA pre-treatment also inhibited the IR-induced increase in intracellular Fe^{2+} levels (Fig. 4C). In addition, 3-MA pretreatment markedly inhibited lipid peroxidation as well as PTGS2 expression, elevated GSH level (Fig. 4D–F), and improved cell viability and clonogenic ability in IR-exposed HIEC cells (Supplementary Figure 1).

A previous study showed that ferritinophagy is mediated by nuclear receptor coactivator 4 (NCOA4) [27]. We found that 6 Gy IR significantly upregulated NCOA4 mRNA and protein expression in the HIEC cells (Fig. 5A and B). In addition, NCOA4 protein expression increased significantly in the small intestines of mice exposed to 14 Gy TAI (Fig. 5C). Endogenous NCOA4 was knocked down using siRNA (Fig. 5D). As shown in Fig. 5D, NCOA4 knockdown inhibited the IR-induced reduction of FTH (Fig. 5D), significantly decreased the level of intracellular free iron (Fig. 5E), and mitigated IR-induced ferroptosis of HIEC cells, as indicated by decreased lipid ROS and PTGS2, and elevated GSH

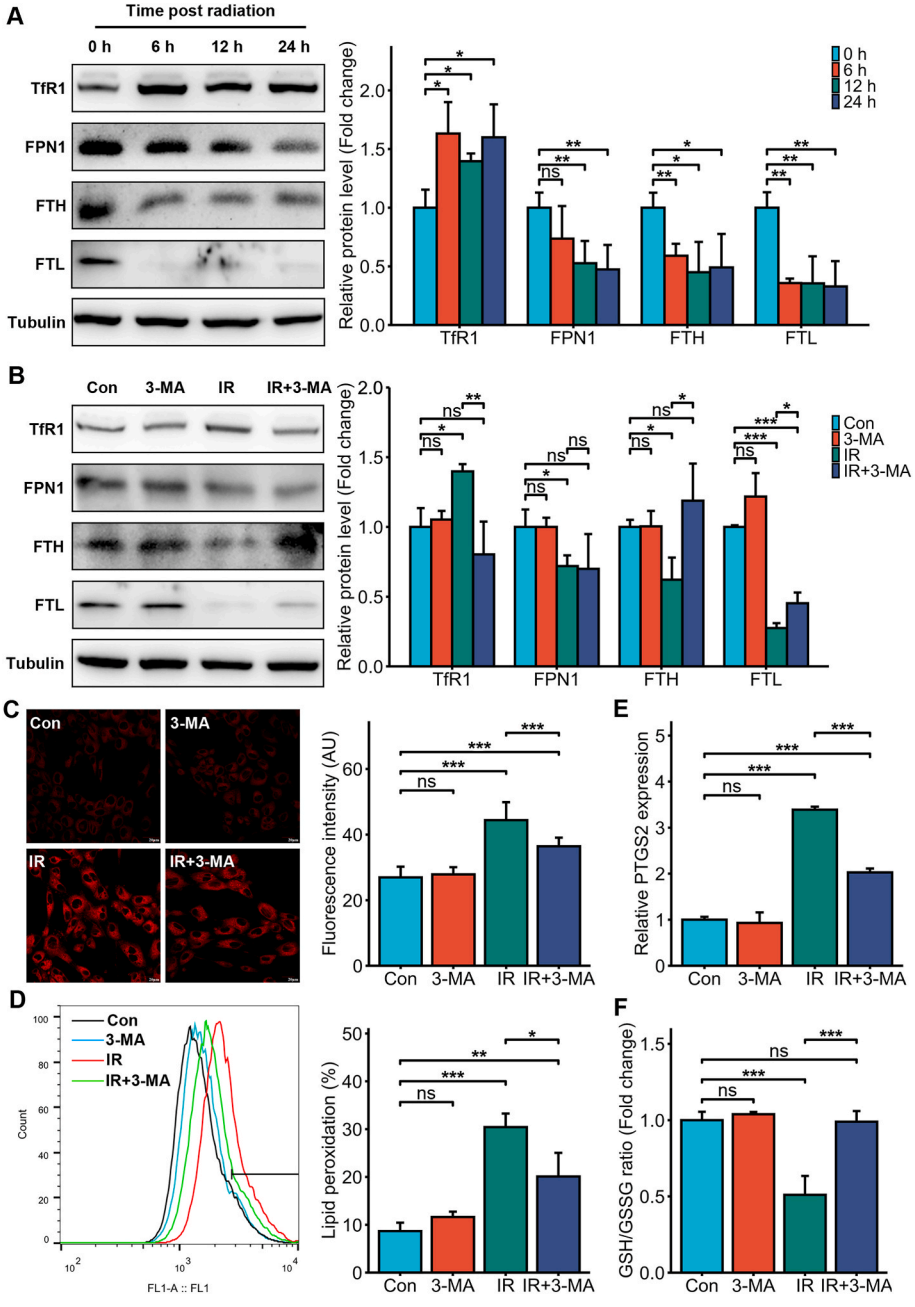

Fig. 4. Autophagy was involved in the intracellular iron overload and ferroptosis induced by IR. (A) Representative immunoblot and quantitative analysis showing the expression levels of TfR1, FPN1, FTH and FTL in the non-irradiated and irradiated (6 Gy) HIEC cells 6, 12 and 24 h post-IR. (B) Representative immunoblot and quantitative analysis showing the expression levels of TfR1, FPN1, FTH and FTL in control or 3-MA (25 μM)-treated HIEC cells after 0 or 6 Gy IR. (C) Representative images of FerroOrange-stained control or 3-MA (25 μM)-treated HIEC cells after 0 or 6 Gy IR showing intracellular Fe^{2+}. Scale bar = 20 μm. Bar graph showing fluorescence intensity in the indicated cells. n = 3 independent experiments. (D) Representative images of C11-BODIPY-stained control or 3-MA (25 μM)-treated HIEC cells after 0 or 6 Gy IR and bar graph showing relative levels of lipid peroxidation in the indicated cells. n = 3 independent experiments. (E) PTGS2 mRNA levels in the control or 3-MA (25 μM)-treated HIEC cells after 0 or 6 Gy IR. n = 3 independent experiments. (F) GSH levels in the control or 3-MA (25 μM)-treated HIEC cells after 0 or 6 Gy IR. n = 3 independent experiments. All data are presented as mean ± S.D. ns, $p \geq 0.05$; *, $p < 0.05$; **, $p < 0.01$; ***, $p < 0.001$.

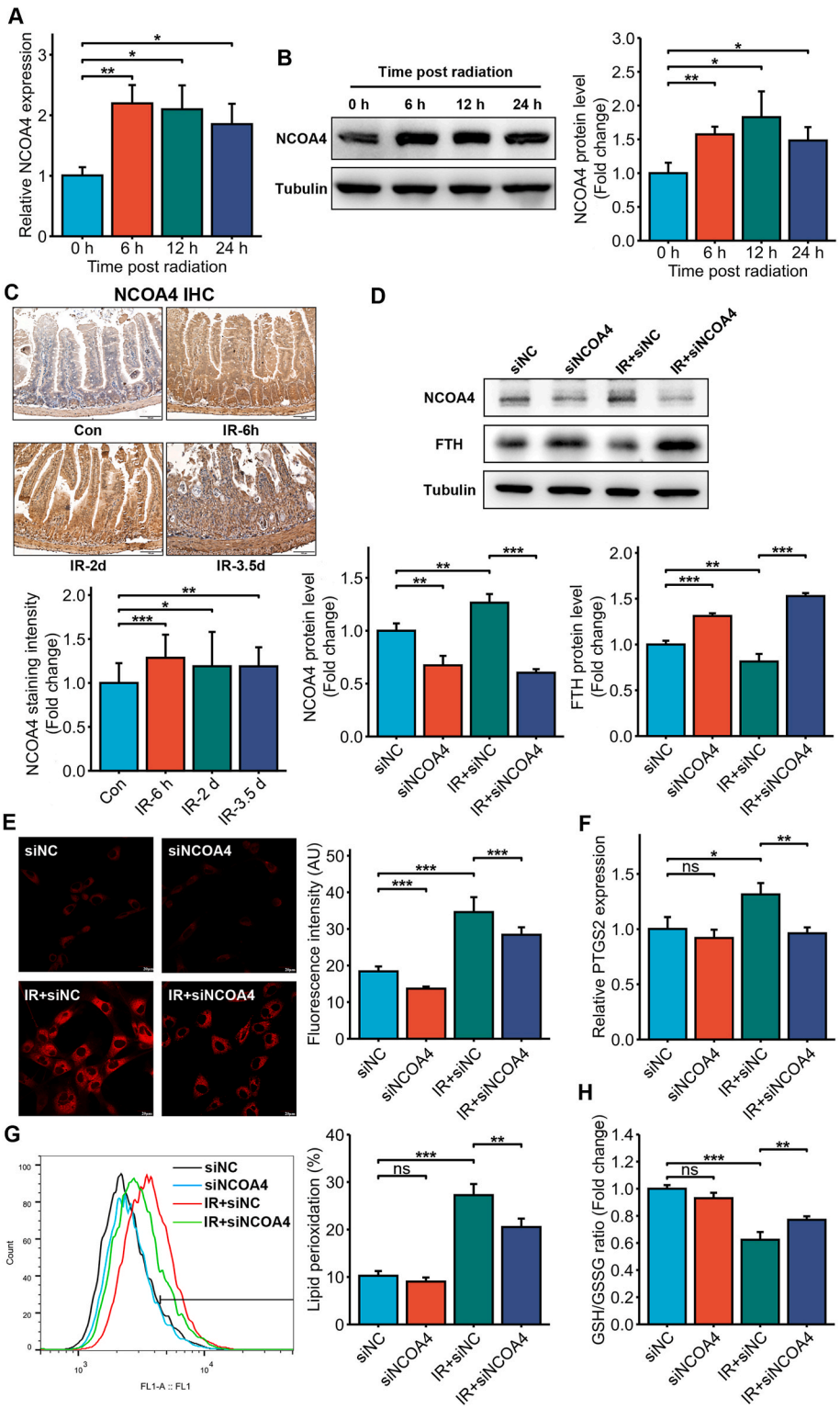

Fig. 5. Ferritinophagy via NCOA4 mediated IR-induced intracellular iron overload and ferroptosis. NCOA4 mRNA (A) and protein (B) expression in the non-irradiated and irradiated (6 Gy) HIEC cells 6, 12 and 24 h post-IR. (C) Representative IHC images and quantitative analysis of intestinal sections of C57BL/6J mice at indicated times after 14 Gy TAI showing NCOA4 expression (Scale bar = 100 μm). (D) NCOA4 and FTH protein levels in siNC or siNCO4 HIEC cells exposed to IR (6 Gy). (E) Representative images of FerroOrange-stained siNC or siNCOA4-treated HIEC cells after 0 or 6 Gy IR showing intracellular Fe^{2+}. Scale bar = 20 μm. Bar graph showing fluorescence intensity in the indicated cells. n = 3 independent experiments. (F) Representative images of C11-BODIPY-stained siNC or siNCOA4-treated HIEC cells after 0 or 6 Gy IR and bar graph showing relative levels of lipid peroxidation in the indicated cells. n = 3 independent experiments. (G) PTGS2 mRNA levels in the siNC or siNCOA4-treated HIEC cells after 0 or 6 Gy IR. n = 3 independent experiments. (H) GSH levels in the siNC or siNCOA4-treated HIEC cells after 0 or 6 Gy IR. n = 3 independent experiments. All data are presented as mean ± S.D. ns, $p \geq 0.05$; *, $p < 0.05$; **, $p < 0.01$; ***, $p < 0.001$.

(Fig. 5F–H). Taken together, IR-mediated intracellular iron overload is driven by NCOA4-mediated ferritinophagy.

3.5. *Intracellular iron overload increased mitochondrial iron levels and dysfunction*

As noted previously, we found that IR resulted in few or absent mitochondrial cristae, and ruptured outer membrane. This raised the possibility that the downstream cellular effects of IR-induced iron overload are mediated by the mitochondria. We observed morphological changes in the mitochondria following IR exposure and DFO treatment, which were categorized as reported previously (for details see materials and methods) [17]. The cells predominantly exhibiting fragmented mitochondria surrounding the nucleus were classified as category III, and those with a network of elongated mitochondria were classified as category I. As Mito-Tracker Red staining indicated, IR exposure led to

extensive mitochondrial fragmentation and peri-nuclear aggregation in the HIEC cells, whereas DFO treatment restored mitochondrial morphology (Fig. 6A and B). Aberrant mitochondrial membrane potential (MMP) is not only a marker of mitochondrial injury but also an early warning sign of ferroptosis [28]. JC-1 staining showed that the MMP was decreased following irradiation, as indicated by higher intensity of the JC-1 monomer (green fluorescence), and membrane depolarization was reversed by DFO treatment (Fig. 6C and D). Furthermore, intracellular ATP levels also dropped significantly after irradiation and were restored by DFO treatment (Fig. 6E), indicating that intracellular iron overload mediates IR-induced mitochondrial dysfunction.

Interestingly, the mitochondrial iron concentration increased significantly following irradiation (Fig. 7A and B), which was accompanied by elevated mitochondrial ROS (Fig. 7C and D). The influx of cytosolic iron and its subsequent storage in the mitochondria are respectively regulated by mitoferrin2 (Mfrn2) and ferritin mitochondrial (Ftmt) [29]. We found that Mfrn2 mRNA was upregulated while Ftmt mRNA was downregulated following irradiation (Fig. 7E and F), suggesting that mitochondrial Fe^{2+} increase may be the result of increased iron input and decreased iron storage. Furthermore, IR-induced Mfrn2 upregulation and Ftmt downregulation were reversed by DFO pre-treatment (Fig. 7E and F), indicating that cytosolic iron mediates the changes of Ftmt and Mfrn2 expression. Mfrn2 expression was inhibited by RNA interference (RNAi) (Fig. 7G). Mfrn2 knockdown significantly decreased the levels of mitochondrial free iron (Fig. 7H and I) and ROS (Fig. 7J and K). Collectively, these results demonstrated that IR-induced cytosolic iron overload increased mitochondrial iron levels and dysfunction.

3.6. Iron-deficient diet mitigated IR-induced intestinal injury in mice

Our findings so far demonstrated that iron plays an important regulatory role in RIII and reducing its levels can protect the intestinal epithelial cells. To assess whether dietary intervention can mitigate RIII, we fed the mice an iron-deficient diet (ID) for 3 weeks (Fig. 8A) and

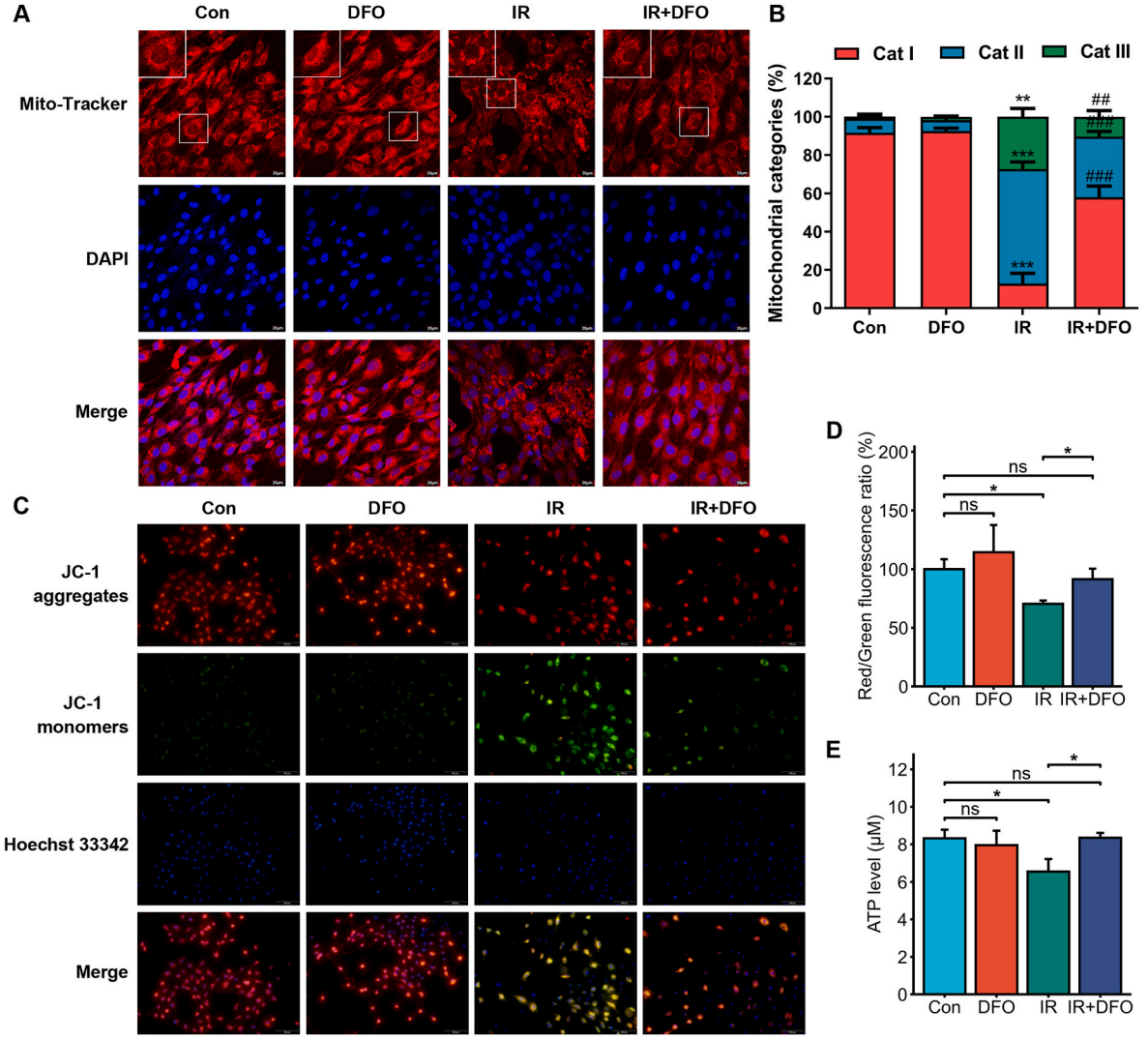

Fig. 6. IR-induced iron overload triggered mitochondrial dysfunction. (A) Representative images of Mito-Tracker-stained control or DFO (500 nM)-treated HIEC cells after 0 or 6 Gy IR showing mitochondrial morphology. The nuclei were counterstained with DAPI. Scale bar = 20 μm. (B) Quantification of 3 categories of mitochondria determined from 400 cells from each treatment group. n = 3 independent experiments. Data are presented as mean ± S.D. **, $p < 0.01$; ***, $p < 0.001$ compared to untreated control; $^{\#\#}$, $p < 0.01$; $^{\#\#\#}$, $p < 0.001$ compared to IR control. (C) Representative images of JC-1-stained control or DFO (500 nM)-treated HIEC cells after 0 or 6 Gy IR showing mitochondrial membrane potential. The nuclei were counterstained with Hoechst 33342. Scale bar = 100 μm. (D) Bar graph showing red/green fluorescence ratio in the indicated cells. n = 3 independent experiments. (E) ATP levels in the control or DFO (500 nM)-treated HIEC cells after 0 or 6 Gy IR. n = 3 independent experiments. All data are presented as mean ± S.D. ns, $p \geq 0.05$; *, $p < 0.05$; **, $p < 0.01$; ***, $p < 0.001$. (For interpretation of the references to colour in this figure legend, the reader is referred to the Web version of this article.)

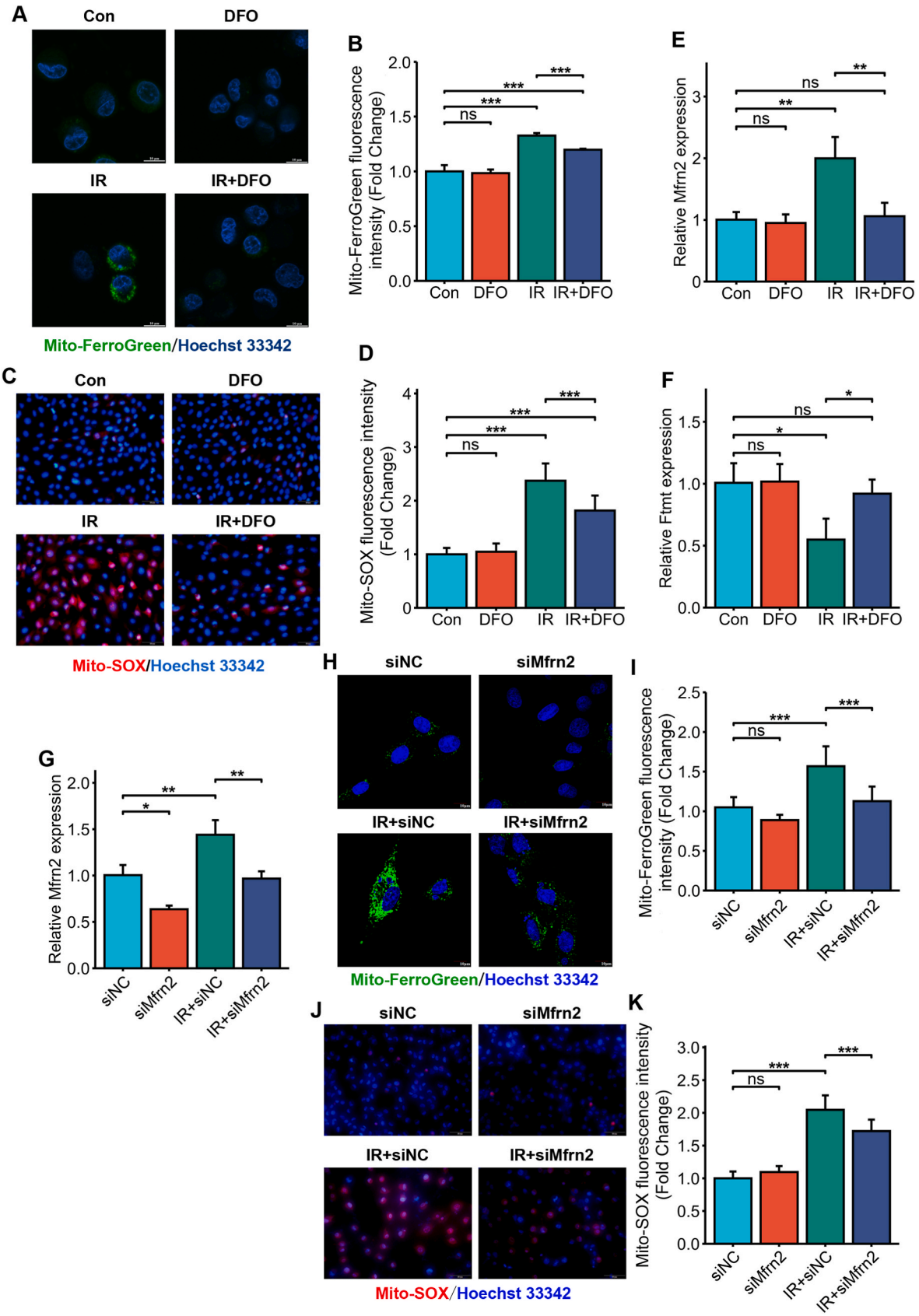

(caption on next page)

Fig. 7. IR-induced iron overload disrupted mitochondrial iron homeostasis. (A) Representative images of Mito-FerroGreen-stained control or DFO (500 nM)-treated HIEC cells after 0 or 6 Gy IR showing mitochondrial Fe^{2+}. The nuclei were counterstained with Hoechst 33342. Scale bar = 10 μm. (B) Bar graph showing fluorescence intensity in the indicated cells. n = 3 independent experiments. (C) Representative images of MitoSox-stained control or DFO (500 nM)-treated HIEC cells after 0 or 6 Gy IR showing mitochondrial ROS generation. The nuclei were counterstained with Hoechst 33342. Scale bar = 50 μm. (D) Bar graph showing fluorescence intensity in the indicated cells. n = 3 independent experiments. Mfrn2 (E) and Ftmt (F) mRNA expression in control or DFO (500 nM)-treated HIEC cells after 0 or 6 Gy IR. n = 3 independent experiments. (G) Mfrn2 mRNA levels in siNC or siMfrn2 HIEC cells exposed to IR (6 Gy). (H) Representative images of Mito-FerroGreen-stained siNC or siMfrn2-treated HIEC cells after 0 or 6 Gy IR showing mitochondrial Fe^{2+}. The nuclei were counterstained with Hoechst 33342. Scale bar = 10 μm. (I) Bar graph showing fluorescence intensity in the indicated cells. n = 3 independent experiments. (J) Representative images of MitoSox-stained siNC or siMfrn2-treated HIEC cells after 0 or 6 Gy IR showing mitochondrial ROS generation. The nuclei were counterstained with Hoechst 33342. Scale bar = 50 μm. (K) Bar graph showing fluorescence intensity in the indicated cells. n = 3 independent experiments. All data are presented as mean ± S.D. ns, $p \geq 0.05$; *, $p < 0.05$; **, $p < 0.01$; ***, $p < 0.001$.

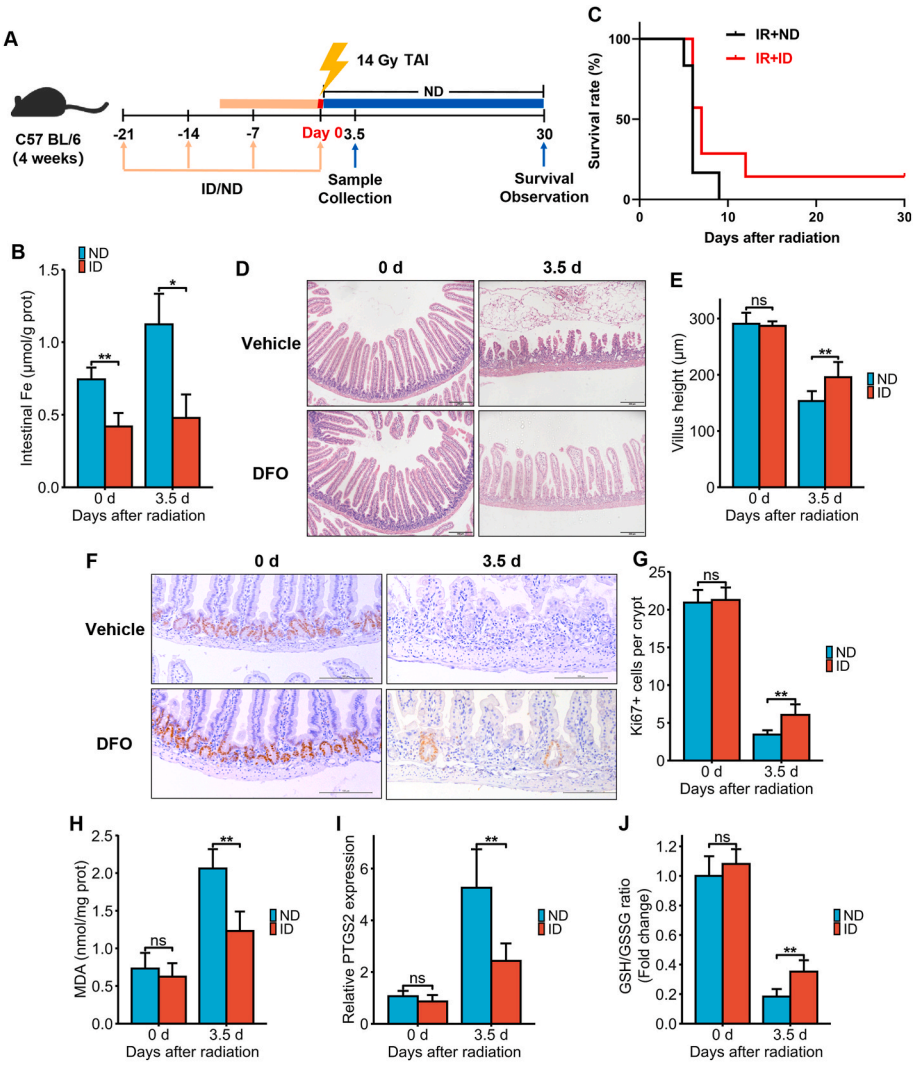

Fig. 8. Iron-deficient diet alleviated IR-induced ferroptosis and intestinal injury in C57BL/6J mice exposed to 14 Gy TAI. (A) Experimental scheme. The mice were fed with an ND or ID diet for 3 weeks and then subjected to 14 Gy TAI. Small intestinal samples were collected 3.5 days post-TAI. Survival of irradiated mice was monitored for up to 30 days post-TAI. (B) Intestinal Fe content of ND or ID-fed mice at days 0 and 3.5 after 14 Gy TAI as determined by ICP-MS. (C) Kaplan-Meier survival analysis of C57BL/6J mice (n = 6 for IR + ND group and n = 7 for IR + ID group). (D) Representative images of H&E-stained intestinal sections from ND or ID-fed mice at days 0 and 3.5 after 14 Gy TAI (Scale bar = 200 μm). (E) Bar graph comparing villus heights in different groups (n = 5/group). All villi around a circumference were measured per sample. (F) Representative IHC images of intestinal sections of ND or ID-fed mice at 3.5 days after TAI showing Ki67 expression (Scale bar = 100 μm). (G) Histograms showing number of $Ki67^{+}$ cells per crypt determined from panel (F) (n = 5/group). Bar graph showing the levels of MDA (H), PTGS2 mRNA (I) and GSH (J) in the small intestinal tissues of C57BL/6J mice at 3.5 days post 14 Gy TAI. n = 5 for each treatment. ND: normal diet; ID: iron-deficient diet. All data are presented as mean ± S.D. ns, $p \geq 0.05$; *, $p < 0.05$; **, $p < 0.01$; ***, $p < 0.001$.

observed a decrease in intestinal iron concentration (Fig. 8B). Long-term ID generally leads to anemia and decreased oxygen-carrying capacity. Since hypoxia can suppress IR-induced injury, we measured the changes of red blood cells (RBC) and hemoglobin (Hb) in the peripheral blood to exclude the possible role of hypoxia in mediating the protective effects of ID. Our results showed that RBC and Hb levels were not significantly different between the normal diet (ND) and ID groups (Supplementary Figure 3), which confirmed that the mice were not anemic and hypoxic after 3 weeks of ID. Both groups were subjected to 14 Gy TAI and monitored for 30 days. As shown in Fig. 8C, ID improved the survival of lethally irradiated mice (IR + ND: 0% *v.s.* IR + ID: 14.3%). Furthermore, the duodenal villus height was similar in both groups prior to irradiation but was significantly greater in the ID group compared to the ND group 3.5 days post-TAI (Fig. 8D and E). Similar trends were observed with the mean number of $Ki67^{+}$ cells in the crypts (Fig. 8F and G), indicating that ID can improve the proliferation rates of small intestinal crypt cells after irradiation. Furthermore, mice in the ID group showed a significant decrease in MDA concentration (Fig. 8H) and PTGS2 mRNA expression (Fig. 8I), and an increase in GSH levels (Fig. 8J) compared to that in the ND group 3.5 days post-TAI. Taken together, an iron-deficient diet can mitigate IR-induced small intestinal cell ferroptosis and thereby RIII.

4. Discussion

Our study demonstrated that iron overload and ferroptosis in the intestinal epithelial cells are the basis of RIII, and can be prevented by

iron chelation or an iron-deficient diet, thus mitigating small intestinal mucosal damage and improving the survival of lethally irradiated mice. Mechanistically, IR promotes ferritinophagy by upregulating NCOA4, which releases free iron that activates Mfrn2 on the mitochondrial membrane of intestinal epithelial cells. Mfrn2-mediated transportation of cytoplasmic free iron into the mitochondria results in mitochondrial iron overload and excessive ROS production, eventually leading to lipid peroxidation and ferroptosis (Fig. 9).

Ferroptosis is a form of cell death caused by iron overload and ROS [8]. IR itself can trigger water radiolysis and substantial ROS generation, resulting in lipid peroxidation and oxidative damage. However, the direct role of iron in IR-induced injury has been rarely reported. Zhang X et al. [10] have shown that IR can increase iron concentration in the bone marrow and serum, leading to ferroptosis of myeloid-macrophage progenitor cells. In fact, post-irradiation iron accumulation in the bone marrow is the primary cause of radiation-induced hemorrhage [10]. Wang L et al. [11] reported that IR can also induce iron overload in the intestinal epithelial cells, although the exact mechanism was not elucidated. Intracellular iron homeostasis depends on the coordination between its input, output and storage, which are respectively regulated by TfR1, FPN1 and ferritin [30]. TfR1 is a transmembrane glycoprotein that internalizes and releases transferrin-bound iron into the cytosol, which is then stored in a non-toxic metalloprotein complex called ferritin, a 24-subunit complex consisting of FTH and FTL. The Fe^{2+} internalized by the intestinal epithelial cells is partly utilized by the cells and partly released through the basement membrane into the blood by both FPN1 and hephaestin. We observed increased TfR1 expression, and a decrease in the expression levels of FPN1, FTL and FTH. This suggested that IR-induced Fe^{2+} overload in the intestinal epithelial cells is likely due to increased iron input, and decreased iron output and storage. A recent study identified TfR1 as a novel marker of ferroptosis [16,31], which was consistent with the post-IR upregulation of TfR1 and increased ferroptosis in intestinal epithelial cells. TfR1 expression usually depends on the cellular iron level and is post-transcriptionally regulated by iron regulatory protein (IRP)1 and IRP2 [32]. In addition, TfR1 is a potential target gene of the endogenous antioxidative stress transcription factor nuclear factor E2-related factor 2 (Nrf2). Our current research focus is to explore the role of these proteins/factors in IR-induced TfR1 upregulation. Furthermore, we found that post-irradiation increase in TfR1 expression was reversed by 3-MA, indicating that it is driven by autophagy. Thus, the mechanism of TfR1 upregulation post-IR is worth further investigation.

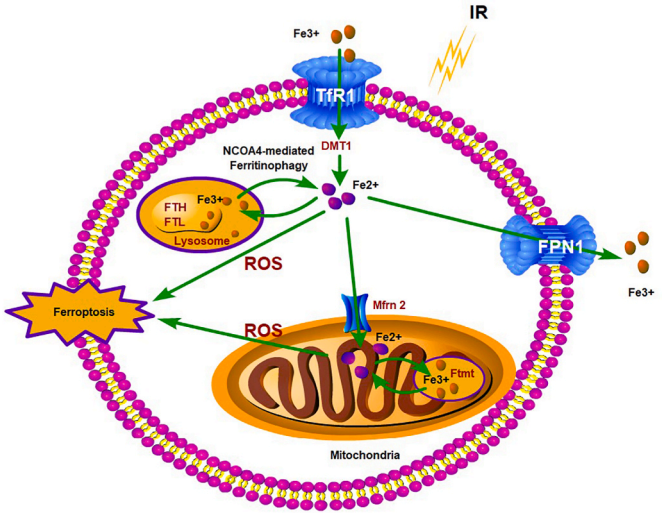

Fig. 9. Schematic representation of the putative mechanism by which IR leads to ferritinophagy and ferroptosis of intestinal epithelial cells. IR promotes ferritinophagy by upregulating NCOA4, which releases free iron that activates Mfrn2 on the mitochondrial membrane of intestinal epithelial cells. Mfrn2-mediated transportation of cytoplasmic free iron into the mitochondria results in mitochondrial iron overload and excessive ROS production, eventually leading to lipid peroxidation and ferroptosis.

Early *in vitro* studies demonstrated that superoxide anions generated by radiation exposure can release Fe^{2+} from ferritin, which generate hydroxyl radicals via the Fenton reaction, eventually leading to lipid peroxidation and oxidative damage [33,34]. We found that 3-MA partially reversed the decrease in ferritin levels and intracellular Fe^{2+} accumulation post-irradiation, suggesting that IR-induced iron overload may be the result of ferritin degradation due to excessive autophagy. Autophagy is a self-catabolic process wherein the lysosomes degrade organelles and proteins in response to stressful stimuli, such as starvation, nutrient deficiency, growth factor deficiency, energy deprivation and IR [35]. It maintains cell metabolism and ensures their survival under stress, and is also critical for internal homeostasis [35]. Ferritinophagy was first described by Mancias et al. [27] in 2014. Using quantitative proteomics, the authors identified NCOA4 as a selective autophagy receptor that mediates ferritin degradation in autophagosomes, which in turn releases the ferritin-bound Fe^{2+} ions. NCOA4 selectively recognizes the FTH subunit of ferritin and binds via FTH R23 [36]. The NCOA4-ferritin complex binds to autophagy related gene (ATG) and thereafter to the primary autophagosome, which then matures into the autophagosome that finally degrades ferritin and releases free iron [36]. Ferritinophagy is closely associated with various physiological and pathological processes including cell growth, proliferation, differentiation, apoptosis and carcinogenesis [37]. Under normal physiological conditions, ferritinophagy is tightly regulated by an iron-dependent protein network to maintain the intracellular Fe^{2+} balance and the related physiological functions. However, excessive ferritinophagy can lead to ferroptosis [37]. Both NCOA4 mRNA and protein were significantly upregulated in the irradiated intestinal epithelial cells, NCOA4 knockdown inhibited the IR-induced reduction of FTH, decreased the level of intracellular free iron and mitigated IR-induced ferroptosis of HIEC cells, which underscores the role of NCOA4-mediated ferritinophagy in IR-induced iron overload and ferroptosis. Ma S et al. [38] demonstrated that radiation increased lysosomal membrane permeabilization and promoted autophagy and the release of lysosomal iron in breast cancer cells, which are also in line with our results. This is the first study to clearly illustrate the exact mechanism of IR-induced iron overload in intestinal epithelial cells, although the mechanistic basis of NCOA4 upregulation still requires further investigation.

Ferroptosis is mainly characterized by increased mitochondrial membrane density, smaller mitochondria, reduced or absent mitochondrial cristae, and outer membrane rupture [7]. Mitochondria are the primary organelles for iron utilization, metabolism and intracellular iron homeostasis [29]. In eukaryotic cells, cytosolic free Fe^{2+} is transported into the mitochondria for heme and iron-sulfur (Fe/S) cluster synthesis [29]. However, the double membrane structure of the mitochondria provides an ideal site for ferroptosis [39]. A previous study showed that erastin failed to induce ferroptosis in mitochondria-deficient cells [40], indicating that mitochondria do indeed play a critical role in ferroptosis [29,41]. Consistent with this, we found that the irradiated HIEC cells had a significant decrease or absence of mitochondrial cristae, along with ruptured outer membrane. Similarly, Wang L et al. [11] observed mitochondrial shrinkage or atrophy, membrane damage, cristae rupture or disappearance, and formation of small mitochondrial vacuoles in the small intestine tissues of mice subjected to 2 Gy total body irradiation. Furthermore, we found that IR significantly altered mitochondrial morphology, decreased MMP, and reduced ATP synthesis in the irradiated HIEC cells. Interestingly, IR-induced mitochondrial damage was alleviated when the endogenous Fe^{2+} was chelated by DFO. IR-induced cytoplasmic Fe^{2+} accumulation also upregulated Mfrn2 and downregulated Ftmt, resulting in increased iron transport and accumulation in the mitochondria, which in turn leads to excessive ROS generation and the aforementioned

mitochondrial dysfunction. Mitochondrial activity is critical for the self-renewal and differentiation of the intestinal stem cells (ISCs) [42], and inhibition of mitochondrial activity in $Lgr5^+$ ISCs impaired intestinal organoid formation [43]. In addition, the $Lgr5^+$ ISCs are required for post-radiation intestinal regeneration [44]. Combined with our findings, we speculate that IR-induced iron overload not only exacerbates RIII but also impairs tissue repair by affecting mitochondrial activity. However, this hypothesis needs further investigation.

The small intestine is the only site of dietary iron absorption, and intestinal iron levels depend on its dietary consumption. Therefore, the dietary iron content may also be critical to the progression of RIII. Studies show that high-iron diet increases oxidative stress, inhibits immune functions, increases the levels of inflammatory cytokines, reduces short-chain fatty acid content in the colon, and enhances the radiosensitivity of the retina and vasculature in rats exposed to long-term low-dose irradiation [45,46]. Although DFO is used for treating disorders associated with systemic iron overload, its clinical application is restricted due to poor lipid solubility, rapid clearance, and treatment-related adverse reactions such as anorexia [47]. The therapeutic effect of regulating the dietary iron consumption on RIII has not been investigated so far. Mice placed on an iron-deficient diet (ID) showed a significant decrease in iron overload and ferroptosis in the small intestine, less mucosal damage and improved survival rate after lethal TAI. Furthermore, 3 weeks of ID feeding did not result in anemia. Our study provides a simple and clinically feasible strategy for the prevention and treatment of RIII.

In summary, we identified an important role of iron in IR-induced ferroptosis and intestinal mucosal damage, elucidated the mechanism by which IR induces iron overload in intestinal epithelial cells, and illustrated the therapeutic effects of iron-based dietary intervention for RIII.

Author contributions statement

ML, YH and ZXW conceived and designed the study. ML guided the project. HZ, YLZ and JAM coordinated and performed most experimental work. LFT and JX performed statistical analyses. ML wrote the manuscript. HY and ZXW provided critical review.

Declaration of competing interest

The authors declare that they have no known competing financial interests or personal relationships that could have appeared to influence the work reported in this paper.

Data availability

Data will be made available on request.

Acknowledgement

This work was supported by the National Natural Science Foundation of China (82192884, 81773356, 81802385), Jiangsu Province Science and Technology Plan Project (BE2018660), Natural Science Foundation of Jiangsu Higher Education Institutions of China (19KJA24000), Suzhou Radiotherapy Clinical Medical Center (Szlcyxzx202103), the Priority Academic Program Development of Jiangsu Higher Education Institutions (PAPD) and Jiangsu Provincial Key Laboratory of Radiation Medicine and Protection.

Appendix A. Supplementary data

Supplementary data to this article can be found online at https://doi.org/10.1016/j.redox.2022.102413.

References

[1] M. Hauer-Jensen, J.W. Denham, H.J. Andreyev, Radiation enteropathy–pathogenesis, treatment and prevention, Nat. Rev. Gastroenterol. Hepatol. 11 (8) (2014) 470–479, https://doi.org/10.1038/nrgastro.2014.46.
[2] L. Lu, W. Li, L. Chen, Q. Su, Y. Wang, Z. Guo, Y. Lu, B. Liu, S. Qin, Radiation-induced intestinal damage: latest molecular and clinical developments, Future Oncol. 15 (35) (2019) 4105–4118, https://doi.org/10.2217/fon-2019-0416.
[3] A. Philchenkov, Radiation-induced cell death: signaling and pharmacological modulation, Crit. Rev. Oncog. 23 (1-2) (2018) 13–37, https://doi.org/10.1615/CritRevOncog.2018026148.
[4] G. Lei, Y. Zhang, P. Koppula, X. Liu, J. Zhang, S.H. Lin, J.A. Ajani, Q. Xiao, Z. Liao, H. Wang, B. Gan, The role of ferroptosis in ionizing radiation-induced cell death and tumor suppression, Cell Res. 30 (2) (2020) 146–162, https://doi.org/10.1038/s41422-019-0263-3.
[5] L.F. Ye, K.R. Chaudhary, F. Zandkarimi, A.D. Harken, C.J. Kinslow, P. S. Upadhyayula, A. Dovas, D.M. Higgins, H. Tan, Y. Zhang, M. Buonanno, T.J. C. Wang, T.K. Hei, J.N. Bruce, P.D. Canoll, S.K. Cheng, B.R. Stockwell, Radiation-induced lipid peroxidation triggers ferroptosis and synergizes with ferroptosis inducers, ACS Chem. Biol. 15 (2) (2020) 469–484, https://doi.org/10.1021/acschembio.9b00939.
[6] S.J. Dixon, K.M. Lemberg, M.R. Lamprecht, R. Skouta, E.M. Zaitsev, C.E. Gleason, D.N. Patel, A.J. Bauer, A.M. Cantley, W.S. Yang, B. Morrison 3rd, B.R. Stockwell, Ferroptosis: an iron-dependent form of nonapoptotic cell death, Cell 149 (5) (2012) 1060–1072, https://doi.org/10.1016/j.cell.2012.03.042.
[7] D. Tang, X. Chen, R. Kang, G. Kroemer, Ferroptosis: molecular mechanisms and health implications, Cell Res. 31 (2) (2021) 107–125, https://doi.org/10.1038/s41422-020-00441-1.
[8] X. Jiang, B.R. Stockwell, M. Conrad, Ferroptosis: mechanisms, biology and role in disease, Nat. Rev. Mol. Cell Biol. 22 (4) (2021) 266–282, https://doi.org/10.1038/s41580-020-00324-8.
[9] X. Li, X. Zhuang, T. Qiao, Role of ferroptosis in the process of acute radiation-induced lung injury in mice, Biochem. Biophys. Res. Commun. 519 (2) (2019) 240–245, https://doi.org/10.1016/j.bbrc.2019.08.165.
[10] X. Zhang, X. Xing, H. Liu, J. Feng, M. Tian, S. Chang, P. Liu, H. Zhang, Ionizing radiation induces ferroptosis in granulocyte-macrophage hematopoietic progenitor cells of murine bone marrow, Int. J. Radiat. Biol. 96 (5) (2020) 584–595, https://doi.org/10.1080/09553002.2020.1708993.
[11] L. Wang, A. Wang, Q. Fu, Z. Shi, X. Chen, Y. Wang, W. Xu, T. Wang, S. Zhang, S. Hu, Ferroptosis plays an important role in promoting ionizing radiation-induced intestinal injuries, Biochem. Biophys. Res. Commun. 595 (2022) 7–13, https://doi.org/10.1016/j.bbrc.2022.01.068.
[12] X. Li, L. Duan, S. Yuan, X. Zhuang, T. Qiao, J. He, Ferroptosis inhibitor alleviates Radiation-induced lung fibrosis (RILF) via down-regulation of TGF-β1, J. Inflamm. 16 (2019) 11, https://doi.org/10.1186/s12950-019-0216-0.
[13] X. Zhang, M. Tian, X. Li, C. Zheng, A. Wang, J. Feng, X. Hu, S. Chang, H. Zhang, Hematopoietic protection and mechanisms of ferrostatin-1 on hematopoietic acute radiation syndrome of mice, Int. J. Radiat. Biol. 97 (4) (2021) 464–473, https://doi.org/10.1080/09553002.2021.1876956.
[14] S. Thermozier, W. Hou, X. Zhang, D. Shields, R. Fisher, H. Bayir, V. Kagan, J. Yu, B. Liu, I. Bahar, M.W. Epperly, P. Wipf, H. Wang, M.S. Huq, J.S. Greenberger, Anti-ferroptosis drug enhances total-body irradiation mitigation by drugs that block Apoptosis and necroptosis, Radiat. Res. 193 (5) (2020) 435–450, https://doi.org/10.1667/RR15486.1.
[15] L.W. Xie, S. Cai, T.S. Zhao, M. Li, Y. Tian, Green tea derivative (-)-epigallocatechin-3-gallate (EGCG) confers protection against ionizing radiation-induced intestinal epithelial cell death both in vitro and in vivo, Free Radic. Biol. Med. 161 (2020) 175–186, https://doi.org/10.1016/j.freeradbiomed.2020.10.012.
[16] G. Lei, Y. Zhang, T. Hong, X. Zhang, X. Liu, C. Mao, Y. Yan, P. Koppula, W. Cheng, A.K. Sood, J. Liu, B. Gan, Ferroptosis as a mechanism to mediate p53 function in tumor radiosensitivity, Oncogene 40 (20) (2021) 3533–3547, https://doi.org/10.1038/s41388-021-01790-w.
[17] J. Grohm, N. Plesnila, C. Culmsee, Bid mediates fission, membrane permeabilization and peri-nuclear accumulation of mitochondria as a prerequisite for oxidative neuronal cell death, Brain Behav. Immun. 24 (5) (2010) 831–838, https://doi.org/10.1016/j.bbi.2009.11.015.
[18] L. Wei, B.J. Leibowitz, X. Wang, M. Epperly, J. Greenberger, L. Zhang, J. Yu, Inhibition of CDK4/6 protects against radiation-induced intestinal injury in mice, J. Clin. Invest. 126 (11) (2016) 4076–4087.
[19] Q. Lu, W. Gong, J. Wang, K. Ji, Y. Wang, C. Xu, Y. Liu, N. He, L. Du, Q. Liu, Identification of circular RNAs altered in mouse Jejuna after radiation, Cell. Physiol. Biochem. 47 (6) (2018) 2558–2568.
[20] M. Li, Y. Gu, Y.C. Ma, Z.F. Shang, C. Wang, F.J. Liu, J.P. Cao, H.J. Wan, X.G. Zhang, Krüppel-like factor 5 promotes epithelial proliferation and DNA damage repair in the intestine of irradiated mice, Int. J. Biol. Sci. 11 (12) (2015) 1458–1468, https://doi.org/10.7150/ijbs.13444.
[21] M. Li, Y. Ma, P. Huang, A. Du, X. Yang, S. Zhang, C. Xing, F. Liu, J. Cao, Lentiviral DDX46 knockdown inhibits growth and induces apoptosis in human colorectal cancer cells, Gene 560 (2) (2015) 237–244, https://doi.org/10.1016/j.gene.2015.02.020.
[22] E.B. Golden, I. Pellicciotta, S. Demaria, M.H. Barcellos-Hoff, S.C. Formenti, The convergence of radiation and immunogenic cell death signaling pathways, Front. Oncol. 2 (2012) 88, https://doi.org/10.3389/fonc.2012.00088.
[23] G. Song, L. Cheng, Y. Chao, K. Yang, Z. Liu, Emerging nanotechnology and advanced materials for cancer radiation therapy, Adv. Mater. 29 (32) (2017), https://doi.org/10.1002/adma.201700996.

[24] J. Huang, Y. Jiang, Y. Ren, Y. Liu, X. Wu, Z. Li, J. Ren, Biomaterials and biosensors in intestinal organoid culture, a progress review, J. Biomed. Mater. Res. 108 (7) (2020) 1501–1508, https://doi.org/10.1002/jbm.a.36921.
[25] M. Gao, P. Monian, Q. Pan, W. Zhang, J. Xiang, X. Jiang, Ferroptosis is an autophagic cell death process, Cell Res. 26 (9) (2016) 1021–1032, https://doi.org/10.1038/cr.2016.95.
[26] W. Hou, Y. Xie, X. Song, X. Sun, M.T. Lotze, H.J. Zeh 3rd, R. Kang, D. Tang, Autophagy promotes ferroptosis by degradation of ferritin, Autophagy 12 (8) (2016) 1425–1428, https://doi.org/10.1080/15548627.2016.1187366.
[27] J.D. Mancias, X. Wang, S.P. Gygi, J.W. Harper, A.C. Kimmelman, Quantitative proteomics identifies NCOA4 as the cargo receptor mediating ferritinophagy, Nature 509 (7498) (2014) 105–109, https://doi.org/10.1038/nature13148.
[28] N. Li, W. Wang, H. Zhou, Q. Wu, M. Duan, C. Liu, H. Wu, W. Deng, D. Shen, Q. Tang, Ferritinophagy-mediated ferroptosis is involved in sepsis-induced cardiac injury, Free Radic. Biol. Med. 160 (2020) 303–318, https://doi.org/10.1016/j.freeradbiomed.2020.08.009.
[29] H. Wang, C. Liu, Y. Zhao, G. Gao, Mitochondria regulation in ferroptosis, Eur. J. Cell Biol. 99 (1) (2020), 151058, https://doi.org/10.1016/j.ejcb.2019.151058.
[30] G. Vigani, Ï.D.M. Solti, S.B. Thomine, K. Philippar, Essential and detrimental - an update on intracellular iron trafficking and homeostasis, Plant Cell Physiol. 60 (7) (2019) 1420–1439, https://doi.org/10.1093/pcp/pcz091.
[31] H. Feng, K. Schorpp, J. Jin, C.E. Yozwiak, B.G. Hoffstrom, A.M. Decker, P. Rajbhandari, M.E. Stokes, H.G. Bender, J.M. Csuka, P.S. Upadhyayula, P. Canoll, K. Uchida, R.K. Soni, K. Hadian, B.R. Stockwell, Transferrin receptor is a specific ferroptosis marker, Cell Rep. 30 (10) (2020) 3411–3423, https://doi.org/10.1016/j.celrep.2020.02.049, e7.
[32] L.C. Kühn, Iron regulatory proteins and their role in controlling iron metabolism, Metallomics 7 (2) (2015) 232–243, https://doi.org/10.1039/c4mt00164h.
[33] M. Aubailly, R. Santus, S. Salmon, Ferrous ion release from ferritin by ultraviolet-A radiations, Photochem. Photobiol. 54 (5) (1991) 769–773, https://doi.org/10.1111/j.1751-1097.1991.tb02088.x.
[34] P. Biemond, H.G. van Eijk, A.J. Swaak, J.F. Koster, Iron mobilization from ferritin by superoxide derived from stimulated polymorphonuclear leukocytes. Possible mechanism in inflammation diseases, J. Clin. Invest. 73 (6) (1984) 1576–1579, https://doi.org/10.1172/JCI111364.
[35] D.J. Klionsky, G. Petroni, R.K. Amaravadi, E.H. Baehrecke, A. Ballabio, P. Boya, J. M. Bravo-San Pedro, K. Cadwell, F. Cecconi, A.M.K. Choi, M.E. Choi, C.T. Chu, P. Codogno, M.I. Colombo, A.M. Cuervo, V. Deretic, I. Dikic, Z. Elazar, E. L. Eskelinen, G.M. Fimia, D.A. Gewirtz, D.R. Green, M. Hansen, M. Jäättelä, T. Johansen, G. Juhász, V. Karantza, C. Kraft, G. Kroemer, N.T. Ktistakis, S. Kumar, C. Lopez-Otin, K.F. Macleod, F. Madeo, J. Martinez, A. Meléndez, N. Mizushima, C. Münz, J.M. Penninger, R.M. Perera, M. Piacentini, F. Reggiori, D.C. Rubinsztein, K.M. Ryan, J. Sadoshima, L. Santambrogio, L. Scorrano, H.U. Simon, A.K. Simon, A. Simonsen, A. Stolz, N. Tavernarakis, S.A. Tooze, T. Yoshimori, J. Yuan, Z. Yue, Q. Zhong, L. Galluzzi, F. Pietrocola, Autophagy in major human diseases, EMBO J. 40 (19) (2021), e108863, https://doi.org/10.15252/embj.2021108863.
[36] J.D. Mancias, L. Pontano Vaites, S. Nissim, D.E. Biancur, A.J. Kim, X. Wang, Y. Liu, W. Goessling, A.C. Kimmelman, J.W. Harper, Ferritinophagy via NCOA4 is required for erythropoiesis and is regulated by iron dependent HERC2-mediated proteolysis, Elife 4 (2015), e10308, https://doi.org/10.7554/eLife.10308.
[37] N. Santana-Codina, J.D. Mancias, The role of NCOA4-mediated ferritinophagy in health and disease, Pharmaceuticals 11 (4) (2018) 114, https://doi.org/10.3390/ph11040114.
[38] S. Ma, X. Fu, L. Liu, Y. Liu, H. Feng, H. Jiang, X. Liu, R. Liu, Z. Liang, M. Li, Z. Tian, B. Hu, Y. Bai, B. Liang, X. Liu, Iron-dependent autophagic cell death induced by radiation in MDA-MB-231 breast cancer cells, Front. Cell Dev. Biol. 9 (2021), 723801, https://doi.org/10.3389/fcell.2021.723801.
[39] N. Sumneang, N. Siri-Angkul, S. Kumfu, S.C. Chattipakorn, N. Chattipakorn, The effects of iron overload on mitochondrial function, mitochondrial dynamics, and ferroptosis in cardiomyocytes, Arch. Biochem. Biophys. 680 (2020), 108241, https://doi.org/10.1016/j.abb.2019.108241.
[40] M. Gao, J. Yi, J. Zhu, A.M. Minikes, P. Monian, C.B. Thompson, X. Jiang, Role of mitochondria in ferroptosis, Mol. Cell 73 (2) (2019) 354–363, https://doi.org/10.1016/j.molcel.2018.10.042, e3.
[41] B. Gan, Mitochondrial regulation of ferroptosis, J. Cell Biol. 220 (9) (2021), e202105043, https://doi.org/10.1083/jcb.202105043.
[42] E. Rath, A. Moschetta, D. Haller, Mitochondrial function - gatekeeper of intestinal epithelial cell homeostasis, Nat. Rev. Gastroenterol. Hepatol. 15 (8) (2018) 497–516, https://doi.org/10.1038/s41575-018-0021-x.
[43] M.J. Rodríguez-Colman, M. Schewe, M. Meerlo, E. Stigter, J. Gerrits, M. Pras-Raves, A. Sacchetti, M. Hornsveld, K.C. Oost, H.J. Snippert, N. Verhoeven-Duif, R. Fodde, B.M. Burgering, Interplay between metabolic identities in the intestinal crypt supports stem cell function, Nature 543 (7645) (2017) 424–427, https://doi.org/10.1038/nature21673.
[44] C. Metcalfe, N.M. Kljavin, R. Ybarra, F.J. de Sauvage, Lgr5+ stem cells are indispensable for radiation-induced intestinal regeneration, Cell Stem Cell 14 (2) (2014) 149–159, https://doi.org/10.1016/j.stem.2013.11.008.
[45] J.L. Morgan, L.E. Ritchie, B.E. Crucian, C. Theriot, H. Wu, C. Sams, S.M. Smith, N. D. Turner, S.R. Zwart, Increased dietary iron and radiation in rats promote oxidative stress, induce localized and systemic immune system responses, and alter colon mucosal environment, Faseb. J. 28 (3) (2014) 1486–1498, https://doi.org/10.1096/fj.13-239418.
[46] C.A. Theriot, C.M. Westby, J.L.L. Morgan, S.R. Zwart, S.B. Zanello, High dietary iron increases oxidative stress and radiosensitivity in the rat retina and vasculature after exposure to fractionated gamma radiation, NPJ Microgravity 2 (2016), 16014, https://doi.org/10.1038/npjmgrav.2016.14.
[47] L.R. Hanson, J.M. Fine, D.B. Renner, A.L. Svitak, R.B. Burns, T.M. Nguyen, N. J. Tuttle, D.L. Marti, S.S. Panter, W.H. Frey 2nd, Intranasal delivery of deferoxamine reduces spatial memory loss in APP/PS1 mice, Drug Deliv. Transl. Res. 2 (3) (2012) 160–168, https://doi.org/10.1007/s13346-011-0050-2.